

Unpaired Deblurring via Decoupled Diffusion Model

Junhao Cheng¹, Wei-Ting Chen², Xi Lu¹, Ming-Hsuan Yang³

¹Sun Yat-sen University ²Microsoft ³University of California, Merced

<https://github.com/donahowe/UID-Diff>

Abstract

Generative diffusion models trained on large-scale datasets have achieved remarkable progress in image synthesis. In favor of their ability to supplement missing details and generate aesthetically pleasing contents, recent works have applied them to image deblurring via training an adapter on blurry-sharp image pairs to provide structural conditions for restoration. However, acquiring substantial amounts of realistic paired data is challenging and costly in real-world scenarios. On the other hand, relying solely on synthetic data often results in overfitting, leading to unsatisfactory performance when confronted with unseen blur patterns. To tackle this issue, we propose UID-Diff, a generative-diffusion-based model designed to enhance deblurring performance on unknown domains by decoupling structural features and blur patterns through joint training on three specially designed tasks. We employ two Q-Formers as structural features and blur patterns extractors separately. The features extracted by them will be used for the supervised deblurring task on synthetic data and the unsupervised blur-transfer task by leveraging unpaired blurred images from the target domain simultaneously. We further introduce a reconstruction task to make the structural features and blur patterns complementary. This blur-decoupled learning process enhances the generalization capabilities of UID-Diff when encountering unknown blur patterns. Experiments on real-world datasets demonstrate that UID-Diff outperforms existing state-of-the-art methods in blur removal and structural preservation in various challenging scenarios.

1 Introduction

Dynamic blur occurs when the camera and subject move relative to each other during the exposure time, resulting in a smeared and blurred image. Deblurring, the process of removing the blur pattern while preserving the underlying structure of degraded images, is essential for restoring high-quality images for human perception and low-level computer vision applications.

With the rapid advancement of photographic technology, a wide range of imaging devices are now employed to capture images in real-world scenarios. Due to their diverse lenses and structural designs, these devices may produce distinct blur patterns [1, 2, 3]. This diversity makes it challenging to develop an all-in-one method for deblurring images from arbitrary and varied sources. Consequently, focusing on deblurring algorithms tailored to specific domains has become increasingly significant.

As deep learning has advanced in recent years, existing deblurring models predominantly build on data-driven approaches that employ neural networks trained via supervised learning on synthetic paired data. Existing works have made efforts to develop deblurring models upon CNN [4, 5], Transformer [6, 7], and GAN [8, 9]. Recently, a new wave of research [10, 11, 12] has begun to investigate the integration of pre-trained generative diffusion models [13], such as Stable Diffusion (SD) [14], with an adapter designed to provide structural guidance for deblurring. These approaches aim to harness the generative capabilities of diffusion models to supplement missing details and generate aesthetically pleasing outputs. However, since paired blurry-sharp training data is limited in

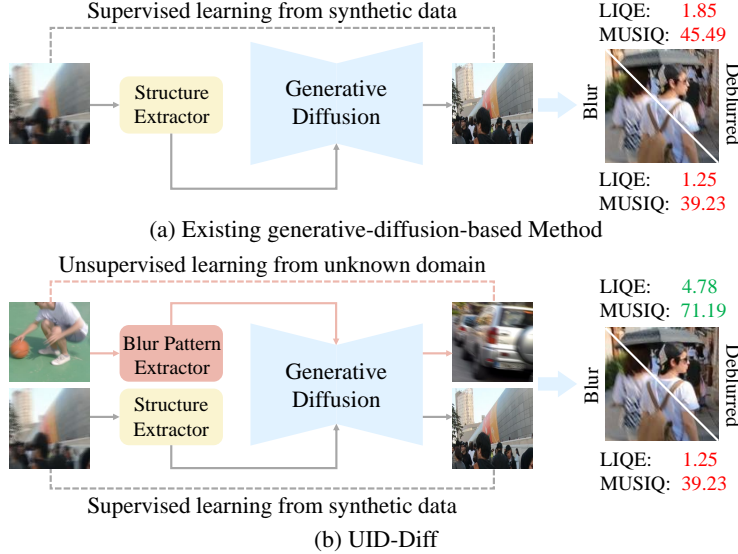


Figure 1: Comparison of UID-Diff with existing generative-diffusion-based deblurring methods. UID-Diff extracts blur patterns from unpaired data to facilitate the supervised structure learning process, thus generalizes well to handle blur images from unknown domains that lack paired data.

practical scenarios, these supervised methods often encounter overfitting issues [2], particularly when dealing with new blur patterns in specific scenarios not captured in the training datasets.

When relying solely on synthetic data is unsuitable, a promising alternative is to develop an unsupervised method that utilizes the unpaired data from a specific domain to perform deblurring directly or serve as an auxiliary for the supervised models. Existing GAN based methods attempt to reproduce the missing fine details [15, 16] or estimate prior knowledge from unpaired data [1, 17, 18, 19]. They are prone to overfitting to a single blur template. Furthermore, they require specific adversarial training [20], which limits their application to diffusion-based models. Other methods [2, 21] try to transfer unseen blur to a certain blur pattern. Unfortunately, these approaches entail additional computational costs and are limited by their inability to conduct large-scale training with a wide variety of synthetic blurs. Consequently, only a few unsupervised approaches for generative-diffusion-based methods have been developed to handle blur images from unknown domains.

In this work, we propose UID-Diff, a generative-diffusion-based model for unpaired image deblurring via blur-decoupled learning. As illustrated in Figure 1, the core concept of UID-Diff lies in its ability to decouple structural features and blur patterns via joint training on supervised structural learning tasks and unsupervised blur pattern learning tasks. Specifically, we employ two Q-Formers [22] to extract the structure and blur pattern separately. The structure extractor is trained on synthetic data to capture structural features from blurry images as conditioning for SD to perform deblurring. Meanwhile, the blur pattern extractor is trained to identify the blur representation of a specific domain by performing unsupervised blur-transfer tasks. In addition, we use a reconstruction task to ensure that the extracted structural features and blur patterns are complementary. As such, UID-Diff generalizes well to handle images from blur domains lacking paired data.

We make the following contributions in this work:

- We present UID-Diff, a generative-diffusion-based model for image deblurring on unknown domains. To the best of our knowledge, this is the first work that integrates the generative diffusion model into unpaired deblurring tasks.
- We introduce an unsupervised learning strategy in the form of the blur-transfer task, which aims to extract blur patterns by leveraging unpaired data from a specific domain, thereby facilitating structure decoupling.
- We propose a joint training strategy to better disentangle the blur pattern and structure features. We prove its effectiveness via experiments on real-world datasets.

2 Related Work

Diffusion Models for Image Restoration. Recent years have witnessed the success of diffusion models in image synthesis [23, 24, 25, 13, 14, 26, 27, 28]. These methods are pre-trained from large-scale text-image pair data [29, 30] and possess strong generative capabilities in producing realistic images and aesthetically pleasing contents [31, 32]. Consequently, some recent works have leveraged these models for image restoration. These approaches can be broadly classified into three paradigms: zero-shot, training from scratch, and training from pre-trained models.

Zero-shot methods [33, 34, 35, 36, 37] leverage pre-trained diffusion models as generative priors. During sampling, they incorporate degraded images as condition to tackle image restoration tasks. However, these methods frequently yield suboptimal results with unpredictable artifacts when applied to real-world data. Other approaches train a conditional diffusion model from scratch [38, 39, 40, 41, 42, 43]. However, they do not possess the advantages of pre-trained Text-to-Image (T2I) diffusion models. In contrast, some recent works have attempted to utilize T2I diffusion models such as Stable Diffusion [14] for image super-resolution [44, 11] and deblurring [45, 10, 12, 46]. These methods train a lightweight adapter to provide structural conditions for restoration. However, when faced with the unpaired deblurring task, limited realistic blurry-sharp image pairs are available for supervised learning. On the other hand, relying solely on synthetic data often leads to overfitting, resulting in unsatisfactory performance when encountering unseen blur patterns. In our work, UID-Diff is developed based on a pre-trained T2I diffusion model and leverages unpaired data for unsupervised blur pattern learning to facilitate the structure extraction process in real-world blur patterns.

Image Deblurring. Image deblurring methods based on deep learning can be broadly categorized into supervised and unsupervised approaches.

Supervised Deblurring with Paired Data. With the advances of deep learning and large-scale synthetic blurry-sharp image pairs [47, 48], supervised learning based approaches attempt to learn the transfer function from the blurry domain to the sharp domain. These methods can be generally categorized into two main types: prior-free and prior-related models. The former attempt to directly develop a robust model for blur removal, leveraging CNNs [49, 50, 51, 52] or Transformers [53, 54, 55, 56]. However, the performance of these methods deteriorates significantly when they encounter unseen blur patterns in real-world scenarios. On the other hand, the latter approaches aim to learn the blur prior to guide the deblurring network. They predict the prior representations through flow based [57, 58] or diffusion based models [59, 60]. Although these approaches achieve improved performance, they cannot learn the prior from unpaired data. This limitation hinders their application in real-world deblurring tasks, where only unpaired data is available.

Unsupervised Deblurring with Unpaired Data. Supervised methods trained on synthetic data often underperform on real-world blur patterns due to overfitting. A promising approach to tackle this issue is by leveraging unpaired data from a specific domain. Some works use unpaired data to perform deblurring directly [16, 1, 17, 18, 19], while use auxiliary tasks to enhance the performance of supervised models [2, 21]. For the first category, some methods restore details in blurry input images by blur-sharp conversion [15, 16]. On the other hand, some models estimate prior knowledge from unpaired data [1, 17, 18, 19, 61]. These approaches usually underestimate the diversity of blur patterns. Furthermore, they require specific adversarial training [20], which limits their application to diffusion based models. While the methods in the second category [2, 21] aim to transfer unknown blur into a certain known blur pattern. Unfortunately, these approaches entail additional computational costs and are limited by their inability to conduct large-scale training with various synthetic blur patterns. In our work, UID-Diff tends to decouple the learning process of structural features and blur patterns to integrate the generative diffusion model into the unpaired deblurring task.

3 Method

3.1 Preliminaries

SD is a type of latent diffusion model [14] that performs a sequence of gradual denoising operations within the latent space and subsequently remaps the denoised latent code into the pixel space to generate the final output image. During the training process, SD initially encodes an input image x into a latent code z using a Variational Auto-Encoder (VAE) [62]. In the subsequent stages, the noisy latent code z_t at timestep t serves as the input for the denoising U-Net ϵ_θ , which interacts with text

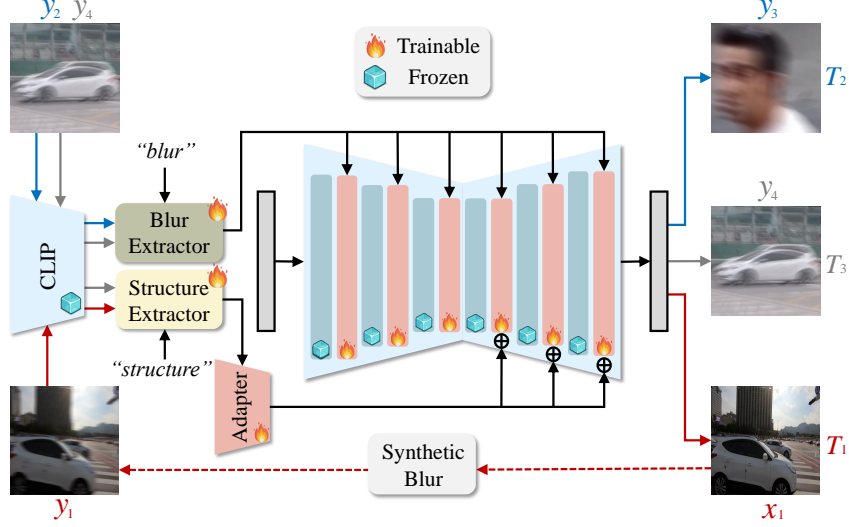


Figure 2: Training pipeline of UID-Diff. UID-Diff achieves blur pattern-structure representation decoupling by joint training on three specific tasks (distinguished by arrows of different colors): 1) The deblurring task, denoted as T_1 , enables the structure extractor to learn structural information from synthetic data; 2) The blur-transfer task, denoted as T_2 , facilitates the blur extractor in learning blur patterns from unpaired blurry images; 3) The reconstruction task, denoted as T_3 , ensures that the extracted structural features and blur patterns are complementary.

condition c via cross-attention. The training objective for this process is defined as follows:

$$\mathcal{L} = \mathbb{E}_{z, c, \epsilon \sim \mathcal{N}(0, 1), t} [\|\epsilon - \epsilon_\theta(z_t, t, c)\|_2^2], \quad (1)$$

where ϵ represents random noise sampled from a standard Gaussian distribution.

3.2 Problem Formulation

Following [2], we formulate a blurry image y as a function of the corresponding sharp image x with underlying structural features f_s through a blur operator $\mathcal{F}_C(\cdot, k)$, which is associated with a device-dependent blur domain C and a blur kernel k :

$$y = \mathcal{F}_C(x, f_s, k) + \eta, \quad (2)$$

where η is a noise term. Our objective is to develop a function \mathcal{G}_C that can extract structural representations from a blurry image $y \in C$. The extracted features will serve as conditions for a pre-trained generative diffusion model SD with an adapter \mathcal{A} to recover the sharp image, i.e.,

$$\begin{aligned} x &= SD[y, \mathcal{A}(f_s), z], \\ f_s &= \mathcal{G}_C(y), \end{aligned} \quad (3)$$

where z is random Gaussian noise. f_s is the structural representation shared by x and y .

3.3 UID-Diff

Q-Former often acts as a representation extractor in conditional image generation [22, 63]. Inspired by this, UID-Diff employs two Q-Formers to separately extract structural features and blur patterns from blurry images as illustrated in Figure 2. These extracted features serve as generation conditions for three specifically designed training tasks, thereby achieving decoupling: 1) The deblurring task (Section 3.4) equips a Q-Former Q_s with the ability to extract structural representation from synthetic data pairs. These features are then sent to an adapter \mathcal{A} to provide restoration condition for SD; 2) The blur-transfer task (Section 3.5) enables another Q-Former Q_b to learn blur patterns from unpaired blurry images within a specific domain; 3) The reconstruction task (Section 3.6) activates both Q_s and Q_b to ensure that the extracted structural and blur features are complementary, thus enabling Q_s to effectively handle images from specific blur domains that lack paired data. For inference (Section 3.7), the Q_s and \mathcal{A} are retained to restore sharp images, as illustrated in Figure 3.

3.4 Deblurring

In SD, additional generation conditions related to image structure, such as sketches and depth maps [64, 65], are often incorporated by adding additional residuals through a ControlNet-like adapter [66, 67]. However, the entanglement of the blur pattern and structural information in the degraded image y makes directly using it as the control signal for \mathcal{A} problematic, as it often leads to instability and produces artifacts [11]. To mitigate these issues, we employ a Q-Former Q_s as a feature extractor to capture the underlying structural features from y .

Denoted as T_1 in Figure 2, we synthesize a blur image y_1 from x_1 and feed y_1 into the CLIP image encoder [68], whose output interacts with the learnable query tokens of Q_s through cross-attention. In this process, we set the word "structure" as the input text for Q_s in anticipation that it can extract features f_s that capture the low-level structure of the image. We follow previous works [12, 11] to employ an adapter \mathcal{A} for UID-Diff. As illustrated in Figure 4, f_s which contains the structural features of y_1 , interacts with the down-sample blocks of \mathcal{A} via cross-attention and is incorporated into the SD U-Net as additional residuals to serve as a structure condition.

The deblurring task is trained non-reconstructive, thus requiring paired blurry-sharp image data. We utilize the method from [47] to synthesize blur to sharp images, thereby creating the necessary paired data for training. The loss function of the deblurring task can be depicted as:

$$\mathcal{L}_1 = \mathbb{E}_{z^{x_1}, c_s, f_s, \epsilon \sim \mathcal{N}(0,1), t} [\|\epsilon - \epsilon_\theta(z_t^{x_1}, c_s, f_s, t)\|_2^2], \quad (4)$$

where $z_t^{x_1}$ is obtained by adding noise to the latent code of x_1 . The text condition c_s is set as "sharp and clean image" for the original text cross-attention of SD.

3.5 Blur-transfer

When the deblurring task is trained solely on synthetic data, it becomes challenging for Q_s to handle images with unseen blur domains C . To address this issue, we employ the blur-transfer task that leverages unpaired blurred images from C to help the model better extract structural features.

In SD, additional generation conditions related to style are typically considered through additional cross attention mechanisms [26, 69]. Inspired by this, we use blur patterns as a special style form. Denoted as T_2 in Figure 2, we employ another Q-Former Q_b to extract f_b that captures the blur pattern of an image $y_2 \in C$. We set the word "blur" as the input text of Q_b to extract representations related to the blur pattern. These representations will be fed into SD through additional cross-attention operations. Specifically, given the query features Z and the text features c , the output of cross-attention Z' from UID-Diff can be defined by the following equation:

$$Z' = \text{Attention}(Q, K, V) + \text{Attention}(Q, K', V'), \quad (5)$$

where $Q = ZW_q$, $K = cW_k$, and $V = cW_v$ are the query, key, and value matrices of the text attention operation, respectively. Here, W_q , W_k , and W_v are the frozen projection matrices. Additionally, $K' = c_b W'_k$ and $V' = c_b W'_v$ are the newly added key and value matrices for the blur-pattern attention operation, respectively, with W'_k and W'_v being the new trainable projection matrices.

The optimization goal of the blur transfer task is to utilize f_b as a blur condition to generate another image $y_3 \in C$, with a different structure but in the same blur domain. The loss function can be depicted as follows:

$$\mathcal{L}_2 = \mathbb{E}_{z^{y_3}, c_b, f_b, \epsilon \sim \mathcal{N}(0,1), t} [\|\epsilon - \epsilon_\theta(z_t^{y_3}, c_b, f_b, t)\|_2^2], \quad (6)$$

where the text condition c_b is set as "blurry image", f_b is the extracted blur features of y_2 , and $z_t^{y_3}$ is obtained by adding noise to the latent code of y_3 . In this way, we anticipate that Q_b can learn to extract unknown blur patterns in an unsupervised paradigm.

3.6 Reconstruction

In the aforementioned two tasks, we use text prompts and a decoupled conditioning mechanism, which allows structure and blur patterns to independently serve as conditions for the diffusion model, to guide the two Q-Formers to focus on their specific tasks. However, there may still be optimization biases. Specifically, Q_s might learn the inverse function of synthetic blur, causing it to still perform poorly in unknown domains. To circumvent this, we employ the reconstruction task, which is

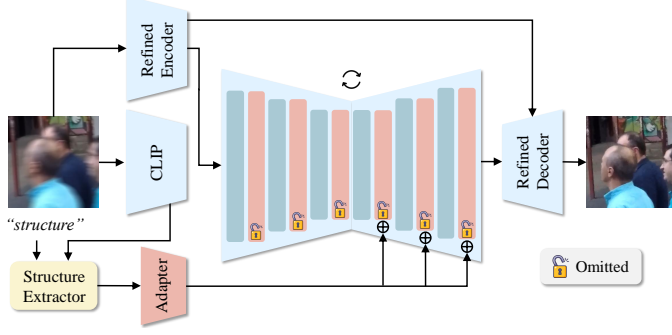


Figure 3: Inference process of UID-Diff. We preserve the Q_s and \mathcal{A} to generate structure guidance, while the newly added cross-attention layer for blur-transfer is omitted.

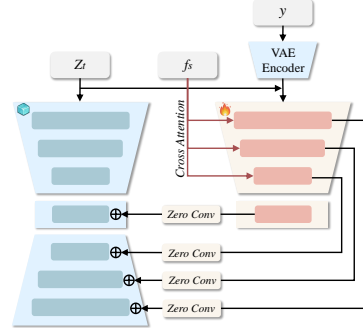


Figure 4: Schematic illustration of the adapter of UID-Diff.

illustrated as T_3 in Figure 2. In this task, Q_s and Q_b are used to extract structure and blur patterns from the same image $y_4 \in C$. These features are simultaneously considered as generation conditions to reconstruct y_4 , with the loss function depicted as:

$$\mathcal{L}_3 = \mathbb{E}_{z^{y_4}, c_b, c_s, f_b, f_c, \epsilon \sim \mathcal{N}(0,1), t} [\|\epsilon - \epsilon_\theta(z_t^{y_4}, c_b, c_s, f_b, f_c, t)\|_2^2], \quad (7)$$

where $z_t^{y_4}$ is obtained by adding noise to the latent code of a blur image from C . This process enables the structure and blur patterns to complement each other, enhancing the generalization capability of Q_s when facing realistic blur patterns.

3.7 Training and Inference

For fast convergence, we first train the deblurring and blur-transfer tasks separately, then incorporate the reconstruction task for joint training. The loss function of the joint training process can be formulated as follows:

$$\mathcal{L} = \alpha \cdot \mathcal{L}_1 + \beta \cdot \mathcal{L}_2 + \gamma \cdot \mathcal{L}_3. \quad (8)$$

Here, \mathcal{L}_1 , \mathcal{L}_2 , and \mathcal{L}_3 represent the loss functions for the deblurring task, the blur-transfer task, and the reconstruction task, respectively; $\alpha + \beta + \gamma = 1$ stands for the sample weights for these three tasks, where we set them to 1:1:1. During the training process, only the Q-Formers, the adapter and the newly added projection metrics are optimized.

The inference process of UID-Diff is illustrated in Figure 3. We retain Q_s and \mathcal{A} to extract structural features, while the newly added cross-attention for the blur-transfer is omitted. We note that SD tends to excessively embellish details, resulting in deviations from the original image. To alleviate this phenomenon, we replace the original SD VAE with a refined-VAE¹, based on previous works [70, 10].

4 Experiments

4.1 Datasets and Metrics

We evaluate our UID-Diff on four widely-used real-world datasets: GoPro [5], RealBlur-J&R [71], and REDS [72]. To emulate real-world deblurring scenarios without paired data, we adhere to existing works [2] to split the training set into distinct blurry subset \mathcal{B} and sharp subset \mathcal{S} . Since generative-diffusion-based methods require large-scale paired data for training, we employ the synthetic blur technique proposed by [71] to generate synthetic blur data \mathcal{B}' from \mathcal{S} , thereby providing adequate blurry-sharp image pairs for supervised training. The statistics of source image sets are reported in Table 2. To effectively evaluate image quality, we include several no-reference image quality assessment (NR-IQA) metrics: MANIQA [73], LIQE [74], MUSIQ [75], and CLIP-IQA [76], which align with prior works [11, 10] for fair comparison².

¹See Appendix A for more details.

²See Appendix B for additional results.

Table 1: Quantitative comparison with SOTA methods on real-world datasets. **Bold** and underlined indicate the best and the second-best performance, respectively.

Data	Metrics	AirNet	PromptIR	FFTformer	AdaRevD	HI-Diff	Blur2Blur	Diff-Plugin	DiffBir	DA-CLIP	Ours
GoPro	MANIQA↑	0.1927	0.2248	0.2736	0.2938	0.2532	0.2321	0.2933	0.3012	0.2873	0.3246
	LIQE↑	1.08	1.06	1.18	1.31	1.13	1.23	1.29	<u>1.24</u>	1.03	1.97
	MSUIQ↑	36.86	36.19	43.11	<u>47.53</u>	39.09	40.31	41.09	<u>50.33</u>	32.06	54.94
	CLIP-IQA↑	0.1904	0.1396	0.1999	0.2831	0.1824	0.2342	0.2458	<u>0.2839</u>	0.1184	0.2978
REDS	MANIQA↑	0.2652	0.3072	0.3602	0.3233	0.2893	0.3342	0.3622	<u>0.3697</u>	0.3526	0.3824
	LIQE↑	1.44	1.86	2.33	2.51	2.43	1.93	2.03	<u>2.51</u>	1.87	2.85
	MSUIQ↑	44.27	54.39	48.34	<u>57.42</u>	58.99	50.32	56.49	<u>59.95</u>	52.57	63.91
	CLIP-IQA↑	0.1980	0.2982	0.4094	<u>0.5903</u>	0.5542	0.2392	0.3968	0.6086	0.2889	0.6086
RealBlur-J	MANIQA↑	0.1896	0.1933	0.2699	0.2603	<u>0.2754</u>	0.2102	0.2513	0.2688	0.2642	0.3092
	LIQE↑	1.07	1.14	1.78	2.07	<u>1.24</u>	1.12	1.17	1.37	1.33	2.11
	MSUIQ↑	41.11	45.23	45.03	<u>41.41</u>	44.42	43.98	45.31	44.85	41.72	47.06
	CLIP-IQA↑	0.1305	0.1749	0.1976	<u>0.2378</u>	0.2217	0.1623	0.1546	0.2098	0.1363	0.2392
RealBlur-R	MANIQA↑	0.2598	0.2731	0.2786	0.3092	0.3113	0.2873	0.3026	0.3198	0.2945	0.3577
	LIQE↑	1.25	1.69	1.88	2.64	2.03	1.67	1.89	<u>2.71</u>	1.12	2.81
	MSUIQ↑	38.19	46.22	42.34	46.63	49.39	40.32	48.43	<u>51.72</u>	21.72	57.19
	CLIP-IQA↑	0.2131	0.2987	0.3984	<u>0.5132</u>	0.4987	0.2451	0.2803	0.4885	0.2761	0.5213

4.2 Implementation Details

We leverage the stable diffusion v1.5 as the pre-trained generative diffusion model. For the image encoder, we employ the ViT-L/14 model from CLIP [68] and set the number of learnable query tokens in the Q-Former to 16, consistent with BLIP-Diffusion [63]. The structural and blur pattern extractors are initialized using the pre-trained weights provided by BLIP-Diffusion

for fast convergence. The training process of UID-Diff includes two phases. First, we train the deblurring and blur-transfer tasks for 50,000 steps as a warm-up. Then, we conduct joint training across all tasks with a 1:1:1 sampling ratio for an additional 500,000 steps. All experiments are executed on NVIDIA A100 GPUs. We utilize the AdamW [77] optimizer with a uniform learning rate of 5×10^{-5} across all training tasks. For the inference phase, we adapt the DDIM sampler [25] with 30 steps to generate outputs. The guidance scale for classifier-free guidance [32] is set to 7.5. Completing all training stages of UID-Diff takes approximately 2 days. During inference, it requires around 20GB of memory on a single A100 GPU and takes about 25 seconds per image.

Table 2: Statistics of data used as unknown domains.

Dataset	Number of data samples			Test
	Sharp (\mathcal{S})	Blur (\mathcal{B})	Synthetic blur (\mathcal{B}')	
GoPro	1261	842	4210	1111
REDS	14400	9600	48000	3000
RealBlur-J	2064	1375	6875	1474
RealBlur-R	2064	1375	6875	1474

4.3 Comparisons with State-of-the-art Methods

In this section, we compare UID-Diff with several SOTA methods, including the generative-diffusion-based approaches DiffBir [11], Diff-Plugin [12], and DA-CLIP [45], as well as other advanced methods: AdaRevD [78], FFTformer [79], HI-Diff [80], PromptIR [6], AirNet [7], and Blur2Blur (unpaired training) [2].

Quantitative Comparisons. The performance comparisons on the test sets of our selected datasets are presented in Table 1. UID-Diff outperforms all baseline models, including the latest unpaired training approach (Blur2Blur) and supervised training generative-diffusion-based method (Diff-Plugin). The results indicate that paired training models exhibit suboptimal performance when faced with unknown domain blur patterns in these real-world datasets. Non-generative-diffusion-based unpaired training method Blur2Blur demonstrates some effectiveness in these scenarios, but it still falls short compared to generative-diffusion-based approaches in most cases. This can be attributed to the capacity of generative diffusion models to generate intricate textures and details through extensive pre-training and aesthetic alignment. Our UID-Diff harnesses the advantages of generative diffusion models and enhances the generalization capability of structure extraction through decoupled training, which results in favorable performance against existing SOTA methods on unpaired deblurring tasks.

Qualitative Comparisons. To assess the visual quality of the results generated by different models, we present their deblurred outputs on the test set of our selected datasets. Figure 5 illustrates the effectiveness of UID-Diff in deblurring across various scenarios, including nighttime, indoor, and wild real-world scenes. On the other hand, existing supervised training methods struggle to remove real blur patterns. In contrast, the performance of the deblurring module limits unpaired training



Figure 5: Visual comparison of deblurring results. UID-Diff outperforms other SOTA methods in real-world deblurring scenarios.

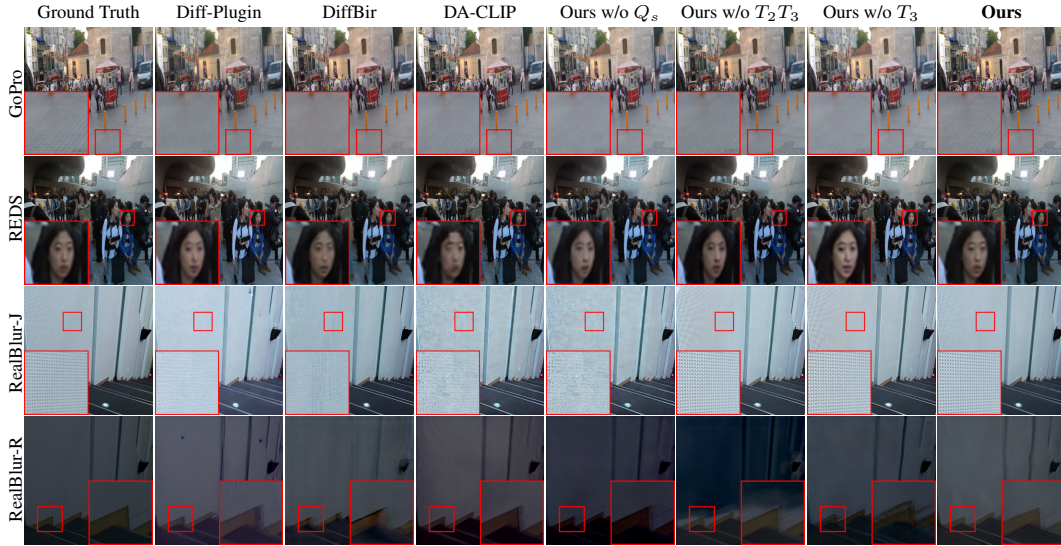


Figure 6: Visual comparison on structural reconstruction. UID-Diff outperforms other generative-diffusion-based methods in preserving fine details.



Figure 7: Deblurring results of ablation studies. Key regions are marked with red boxes and magnified.

methods and fails to achieve satisfactory visual results. We observe that using inappropriate features as input for generative-diffusion-based methods may lead to artifacts and distortions. Based on this, we compare the structure reconstruction performance of UID-Diff with existing supervised generative-diffusion-based methods and with three variants³ of our model that only processes supervised training. As demonstrated in Figure 6, UID-Diff performs favorably in reconstructing detailed structures such as facial features, text, and intricate patterns. In contrast, other supervised diffusion-based methods struggle to effectively decouple structure and blur patterns in real-world scenarios, resulting in distortions and artifacts in the restored images. Please refer to Appendix C for more visual results.

³Detailed in Section 4.4.

Table 3: Results of ablation study.

Dataset	Model	Components			Training Tasks			Metrics			
		Q_s	Q_b	r-VAE	T_1	T_2	T_3	MANIQA \uparrow	LIQE \uparrow	MUSIQ \uparrow	CLIP-IQA \uparrow
GoPro	w/o Q_s	\times	\times	\checkmark	\checkmark	\times	\times	0.2797	1.29	41.22	0.2469
	w/o T_2T_3	\checkmark	\times	\checkmark	\checkmark	\times	\times	0.2933	1.91	52.33	0.2599
	w/o T_3	\checkmark	\checkmark	\checkmark	\checkmark	\checkmark	\times	0.3124	1.95	50.88	0.2659
	w/o r-VAE	\checkmark	\checkmark	\times	\checkmark	\checkmark	\checkmark	0.3240	1.86	54.69	0.2966
	Ours	\checkmark	\checkmark	\checkmark	\checkmark	\checkmark	\checkmark	0.3246	1.97	54.94	0.2978
REDS	w/o Q_s	\times	\times	\checkmark	\checkmark	\times	\times	0.3698	2.33	57.05	0.4003
	w/o T_2T_3	\checkmark	\times	\checkmark	\checkmark	\times	\times	0.3703	1.91	54.15	0.3433
	w/o T_3	\checkmark	\checkmark	\checkmark	\checkmark	\checkmark	\times	0.3729	2.23	61.89	0.5402
	w/o r-VAE	\checkmark	\checkmark	\times	\checkmark	\checkmark	\checkmark	0.3817	2.81	63.52	0.6066
	Ours	\checkmark	\checkmark	\checkmark	\checkmark	\checkmark	\checkmark	0.3824	2.85	63.91	0.6086
RealBlur-J	w/o Q_s	\times	\times	\checkmark	\checkmark	\times	\times	0.2705	1.16	25.58	0.1633
	w/o T_2T_3	\checkmark	\times	\checkmark	\checkmark	\times	\times	0.2823	1.40	20.98	0.1993
	w/o T_3	\checkmark	\checkmark	\checkmark	\checkmark	\checkmark	\times	0.2905	1.54	24.71	0.2092
	w/o r-VAE	\checkmark	\checkmark	\times	\checkmark	\checkmark	\checkmark	0.3024	2.05	26.96	0.2390
	Ours	\checkmark	\checkmark	\checkmark	\checkmark	\checkmark	\checkmark	0.3092	2.11	27.06	0.2392
RealBlur-R	w/o Q_s	\times	\times	\checkmark	\checkmark	\times	\times	0.3289	1.94	48.41	0.2925
	w/o T_2T_3	\checkmark	\times	\checkmark	\checkmark	\times	\times	0.3401	1.44	40.98	0.2392
	w/o T_3	\checkmark	\checkmark	\checkmark	\checkmark	\checkmark	\times	0.3485	2.11	47.19	0.4013
	w/o r-VAE	\checkmark	\checkmark	\times	\checkmark	\checkmark	\checkmark	0.3574	2.73	57.11	0.5210
	Ours	\checkmark	\checkmark	\checkmark	\checkmark	\checkmark	\checkmark	0.3577	2.81	57.19	0.5213

4.4 Ablation Study

In this section, we explore the effectiveness of each key component and training phase of UID-Diff. All ablation studies are conducted under the same settings as described in Section 4.2.

Effectiveness of Reconstruction. We perform ablation by removing the reconstruction task during the joint training phase, denoted as "w/o T_3 ". The quantitative results presented in Table 3 and qualitative results shown in Figure 6 and Figure 7 indicate that omitting the reconstruction task results in decline in both quantitative metrics and visual quality. This underscores the importance of the reconstruction task in enhancing the complementarity between structural features and blur patterns, thus improve the generalization ability of Q_s .

Effectiveness of Blur-transfer. We conduct ablation studies to evaluate the effectiveness of the blur-transfer task by removing the joint-training phase, denoted as "w/o T_2T_3 ". As illustrated in Table 3, Figure 6 and Figure 7, training the deblurring task solely on synthetic data is insufficient to handle unknown domain blurs, resulting in decline in both quantitative results and visual quality. This is because the structure extractor overfits synthetic blur patterns and fails to decouple unseen blur patterns in real-world scenarios effectively. We further validate the effectiveness of the blur pattern extractor Q_b by visualizing the blur-transfer results in Appendix C.

Effectiveness of the Structure Extractor. We investigate the impact of the structure extractor Q_s by removing it in the deblurring task, denoted as "w/o Q_s ". As demonstrated in Table 3, the absence of Q_s results in a performance decline across all datasets. Figure 6 and Figure 7 reveal the emergence of artifacts and distortions when Q_s is removed, underscoring its importance in eliminating features unrelated to structural information to enhance the quality of the restored output.

Ablation on the refined-VAE. We conduct an ablation study by replacing the refined-VAE with the original SD VAE, denoted as "w/o r-VAE". As shown in Table 3, using the original VAE results in a slight performance drop in no-reference metrics; however, UID-Diff with the original VAE still outperforms all baseline methods. The visual results presented in Figure 7 indicate that UID-Diff with the refined-VAE effectively mitigates deviations from the original image.

5 Conclusion

In this work, we propose UID-Diff, a generative-diffusion-based model for unpaired image deblurring via blur-decoupled learning. By joint training on a supervised deblurring task, an unsupervised blur pattern learning task, and a reconstruction task, UID-Diff generalizes well to handle images from unknown domains that lack paired data. Experiments on widely-used real-world datasets demonstrate that UID-Diff outperforms existing SOTA methods in blur removal and structural preservation, showcasing its potential for application in diverse and challenging environments.

Appendix

The outline of the Appendix is as follows:

- Details of the refined-VAE in UID-Diff.
- Additional quantitative results.
- Additional qualitative results.
- Broader Impact.

A Details of the Refined-VAE in UID-Diff

In this section, we introduce the refined-VAE in UID-Diff. The pre-trained SD model utilizes a VAE to compress images into latent codes, reducing computational costs during diffusion. However, due to the compression inherent in the VAE and the randomness of the diffusion process, using the original SD VAE in deblurring tasks can lead to issues such as detail distortion and loss, resulting in discrepancies between the restored images and the input ones [81]. To mitigate this issue, we replace the VAE of SD with a refined-VAE, consistent with previous generative-diffusion-based methods [10, 70]. As illustrated in Figure 8, the refined-VAE \mathcal{V}' introduces feature constraints by adding a refiner to both the encoder and decoder of the original VAE \mathcal{V} to align the compressed latent codes and the input images. The encoder refiner performs pre-filtering operations on the degraded features after each layer of the original VAE encoder, thereby reducing content loss during compression. These refined features are then combined with the decoder-refiner via skip connections. The decoder refiner operates after each decoder layer of the original VAE, aiming to combine the features of the original image when decoding the latent codes refined by the diffusion process. This approach helps to minimize the discrepancies between the decoded image and the original one.

During training, we adapt the strategy from [70], which consists of two phases. In the first phase, we train the encoder refiner. The degraded image y is encoded into latent codes using \mathcal{V}' , while the corresponding sharp image x is encoded into ground truth latent codes using \mathcal{V} . The Mean Squared Error (MSE) loss is used for constraint. The optimization function is as follows:

$$\mathcal{L}_{\text{encoder}} = \text{MSE}(\mathcal{V}(x), \mathcal{V}'\text{encoder}(x)). \quad (9)$$

In the second phase, we train the decoder refiner. We freeze the trained encoder refiner and utilize $\mathcal{V}'_{\text{encoder}}$ to encode x into latent codes z with intermediate features. The trained UID-Diff then processes z to generate the final latent codes, which will be decoded into images using the refined VAE decoder $\mathcal{V}'_{\text{decoder}}$, considering the intermediate features. The generated image is compared with the corresponding sharp image x using MSE loss. The optimization function is as follows:

$$\begin{aligned} \mathcal{L}_{\text{decoder}} &= \text{MSE}(x, \mathcal{V}'\text{decoder}(\text{UID-Diff}(z))), \\ z &= \mathcal{V}'\text{encoder}(y). \end{aligned} \quad (10)$$

For fast convergence, the parameters of the original VAE are frozen during the training process. We use the same method as described in Section 4.2 to construct synthetic data for training the refiner to ensure fair comparison.

B Additional Quantitative Results

In this section, we present additional quantitative results on reference-based metrics: FID, PSNR, SSIM, and LPIPS [82]. All experimental settings are aligned with Section 4.

Comparison with SOTA Methods. The performance comparisons with selected baselines on reference-based metrics are presented in Table 4. UID-Diff performs favorably against other generative-diffusion-based methods across all selected datasets. Notably, due to the generative nature of T2I diffusion models and the randomness of the diffusion process, generative-diffusion-based methods tend to supplement details in blurred regions at the expense of consistency with the original image. As a result, they generally underperform on reference-based metrics compared to non-diffusion-based models. However, the decoupled learning strategy of UID-Diff allows it to effectively extract structural information from blurred images and restore structures that are faithful to the original image, thereby maintaining competitiveness with other SOTA methods.

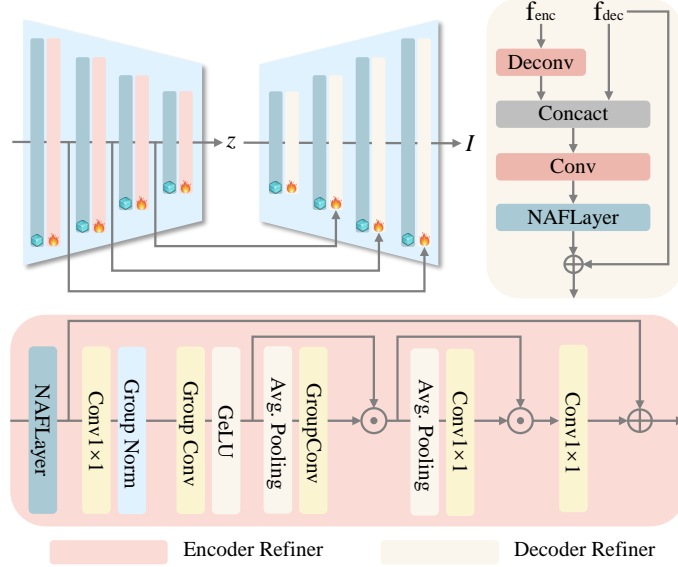


Figure 8: Architecture of the refined-VAE in UID-Diff.

Table 4: Ablation study results on reference-based metrics.

Dataset	Model	Components			Training Tasks			Metrics			
		Q_s	Q_b	r-VAE	T_1	T_2	T_3	FID↓	PSNR↑	SSIM↑	LPIPS↓
GoPro	w/o Q_s	✗	✗	✓	✓	✗	✗	50.52	22.67	0.6887	0.1689
	w/o T_2T_3	✓	✗	✓	✓	✗	✗	54.53	22.91	0.7316	0.1541
	w/o T_3	✓	✓	✓	✓	✓	✗	50.45	24.34	0.7231	0.1552
	w/o r-VAE	✓	✓	✗	✓	✓	✓	50.37	23.96	0.6984	0.1563
	Ours	✓	✓	✓	✓	✓	✓	49.68	25.08	0.7403	0.1310
REDS	w/o Q_s	✗	✗	✓	✓	✗	✗	26.86	22.03	0.6210	0.0783
	w/o T_2T_3	✓	✗	✓	✓	✗	✗	27.22	23.53	0.6871	0.0782
	w/o T_3	✓	✓	✓	✓	✓	✗	30.03	23.60	0.7137	0.0813
	w/o r-VAE	✓	✓	✗	✓	✓	✓	28.88	23.36	0.7223	0.1687
	Ours	✓	✓	✓	✓	✓	✓	26.35	25.83	0.7782	0.0682
RealBlur-J	w/o Q_s	✗	✗	✓	✓	✗	✗	38.92	18.93	0.5283	0.2090
	w/o T_2T_3	✓	✗	✓	✓	✗	✗	38.98	21.27	0.7283	0.2257
	w/o T_3	✓	✓	✓	✓	✓	✗	38.94	21.33	0.7205	0.2170
	w/o r-VAE	✓	✓	✗	✓	✓	✓	38.78	20.63	0.7189	0.1544
	Ours	✓	✓	✓	✓	✓	✓	37.99	22.76	0.7293	0.1379
RealBlur-R	w/o Q_s	✗	✗	✓	✓	✗	✗	37.44	16.21	0.5213	0.2501
	w/o T_2T_3	✓	✗	✓	✓	✗	✗	37.08	17.27	0.5283	0.2457
	w/o T_3	✓	✓	✓	✓	✓	✗	34.49	19.74	0.5345	0.2458
	w/o r-VAE	✓	✓	✗	✓	✓	✓	33.74	21.84	0.5104	0.2563
	Ours	✓	✓	✓	✓	✓	✓	32.11	22.47	0.5387	0.2348

Ablation Study. The results of the ablation study on reference-based metrics are presented in Table 4. Omitting any key component or training phase from UID-Diff leads to a decline across all reference-based metrics, which aligns with the performance trend observed in the NR-IQA metrics shown in Table 3 in the main paper. This further demonstrates the effectiveness of UID-Diff.

C Additional Qualitative Results

Blur-transfer Visualization. In addition to the quantitative results that demonstrate the effectiveness of the blur-transfer task, we further evaluate the performance of the blur pattern extractor Q_b by visualizing the blur-transfer outputs. We randomly select a sharp image a and a blurred image b

from the test sets. We encode b into a latent code and perform diffusion sampling conditioned on the extracted blur pattern of a . The results in Figure 9 and Figure 10 demonstrate that Q_b successfully captures and transfers the blur patterns from a to b . Although the blur-transfer result c does not achieve pixel-level correspondence with b due to the randomness of the diffusion process, c remains independent of the structure of a . This indicates that Q_b has been effectively trained to extract only the blur pattern. On the other hand, Q_s can focus on extracting the complementary structural features.

Deblurring Visualization. In this section, we present additional visualization results on the test sets of our selected datasets: GoPro, REDS, RealBlur-J & R. As shown in Figure 11 and Figure 18, UID-Diff performs favorably against other SOTA methods across various real-world deblurring scenarios.

D Broader Impact

The proposed UID-Diff contributes to advancing the field of image deblurring by introducing generative-diffusion-model into unpaired deblurring task. Its ability to generalize across diverse domains has potential applications in areas that lack paired data for supervised training.

However, the deployment of generative diffusion models in image deblurring also raises certain ethical considerations. The ability to manipulate images could be misused for deceptive purposes, such as altering visual evidence or creating misleading content. Researchers and practitioners should evaluate the societal implications and ensure that their deployment aligns with ethical guidelines.

Table 5: Quantitative comparison with SOTA methods on reference-based metrics. **Bold** and underlined indicate the best and the second-best performance, respectively.

Data	Metrics	AirNet	PromptIR	FFTformer	AdaRevD	HI-Diff	Blur2Blur	Diff-Plugin	DiffBir	DA-CLIP	Ours
GoPro	FID↓	56.09	49.65	48.74	31.92	59.32	46.31	<u>50.55</u>	58.45	54.79	49.68
	PSNR↑	21.82	21.97	22.21	26.93	23.46	24.33	<u>22.87</u>	23.42	<u>24.24</u>	25.08
	SSIM↑	0.7348	0.7361	0.6843	0.7492	0.7304	0.7392	0.6902	<u>0.7043</u>	0.6442	0.7403
	LPIPS↓	0.1446	0.1390	0.1187	0.0893	0.1293	0.1317	0.1388	0.1382	0.1299	<u>0.1310</u>
REDS	FID↓	33.36	16.57	12.84	14.74	13.75	15.49	<u>26.80</u>	37.19	62.14	15.35
	PSNR↑	23.94	27.03	27.53	28.78	24.77	28.94	<u>21.95</u>	<u>22.67</u>	21.43	25.48
	SSIM↑	0.7419	0.8149	0.8320	0.8623	0.8132	0.8522	<u>0.6215</u>	<u>0.5714</u>	0.5953	0.7822
	LPIPS↓	0.0975	0.0504	0.0498	0.0231	0.0510	0.0431	<u>0.0773</u>	0.0817	0.1402	0.0498
RealBlur-J	FID↓	38.52	17.02	15.43	16.53	16.23	16.64	<u>38.68</u>	48.29	52.61	17.99
	PSNR↑	22.51	22.51	25.52	27.95	21.53	22.71	<u>22.61</u>	22.76	22.35	22.76
	SSIM↑	0.7347	0.7598	0.7622	0.8531	0.7523	0.7642	<u>0.7035</u>	<u>0.7220</u>	0.7129	0.7693
	LPIPS↓	0.1483	0.1382	0.1135	0.1352	0.1346	0.1314	0.1568	<u>0.1471</u>	0.1794	0.1379
RealBlur-R	FID↓	40.93	36.82	35.94	40.35	28.87	21.43	<u>35.91</u>	38.33	92.61	32.11
	PSNR↑	16.82	17.03	26.94	27.85	21.02	19.82	16.56	17.24	21.35	22.47
	SSIM↑	0.5093	0.5290	0.7542	0.8034	0.7099	0.5432	0.5206	0.4883	<u>0.7129</u>	0.7384
	LPIPS↓	0.2295	0.2011	0.1790	0.1872	0.2093	0.2231	<u>0.2147</u>	0.2107	0.2794	0.2348



Figure 9: Visualization of blur transferring. The blur pattern in the images of the first row is transferred to the images in the second row to generate the blurred output in the third row.

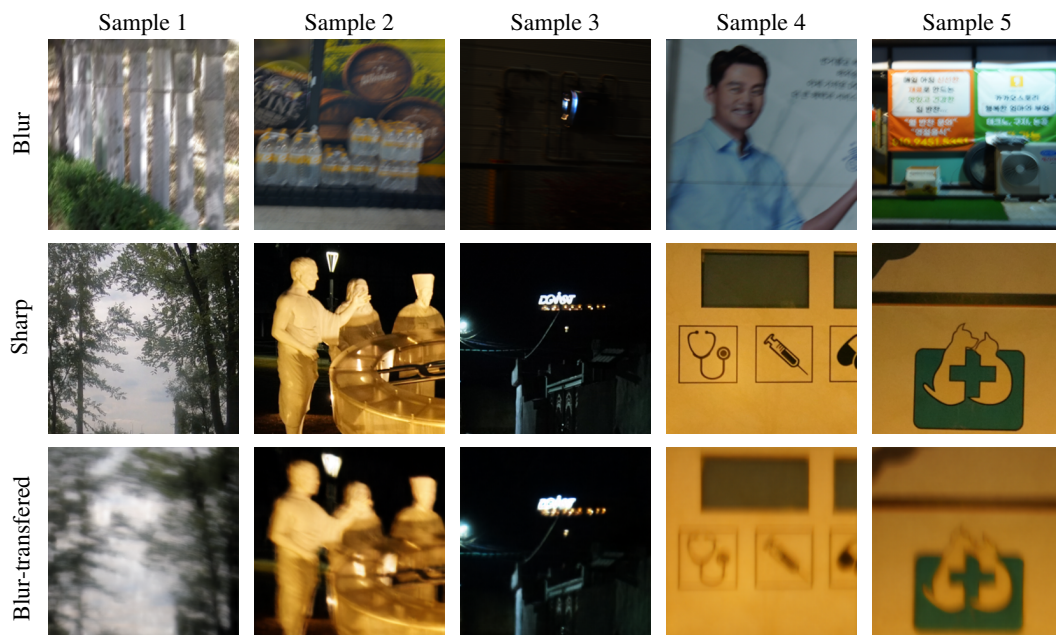


Figure 10: Visualization of blur transferring. The blur pattern in the images of the first row is transferred to the images in the second row to generate the blurred output in the third row.



Figure 11: Additional visual comparison on the **GoPro** dataset.

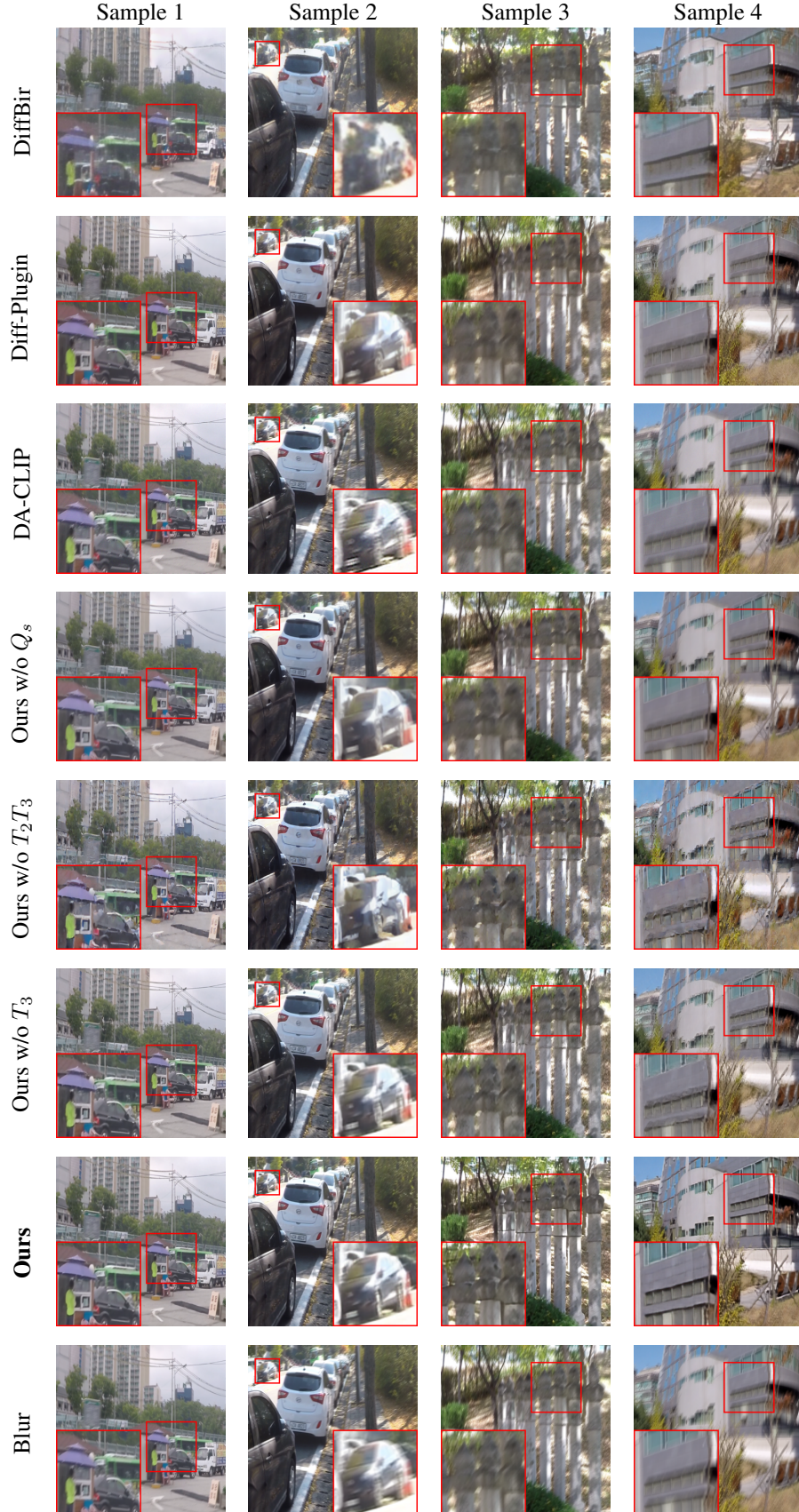


Figure 12: Additional visual comparison on the GoPro dataset (Continue).

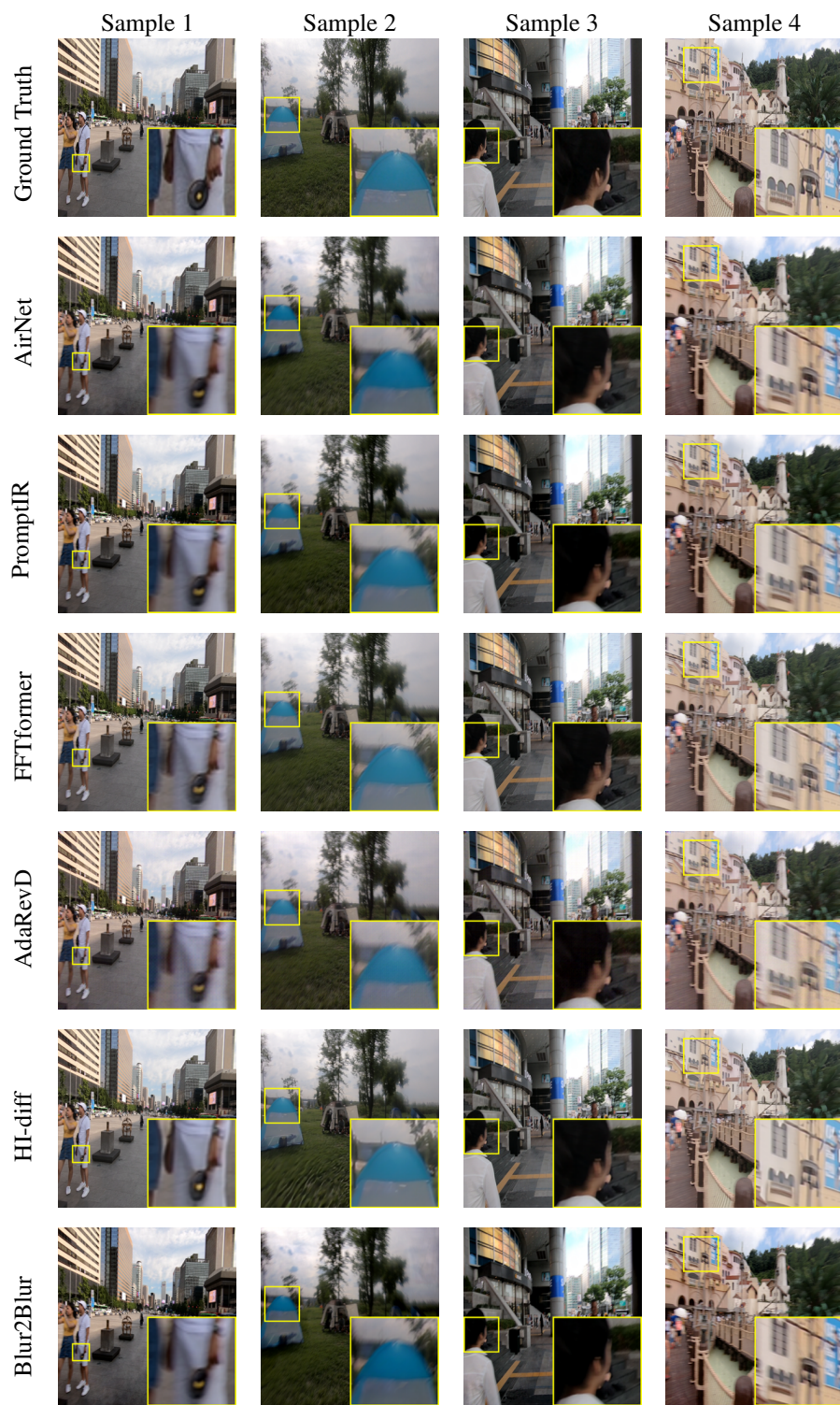


Figure 13: Additional visual comparison on the REDS dataset.



Figure 14: Additional visual comparison on the REDS dataset (Continue).

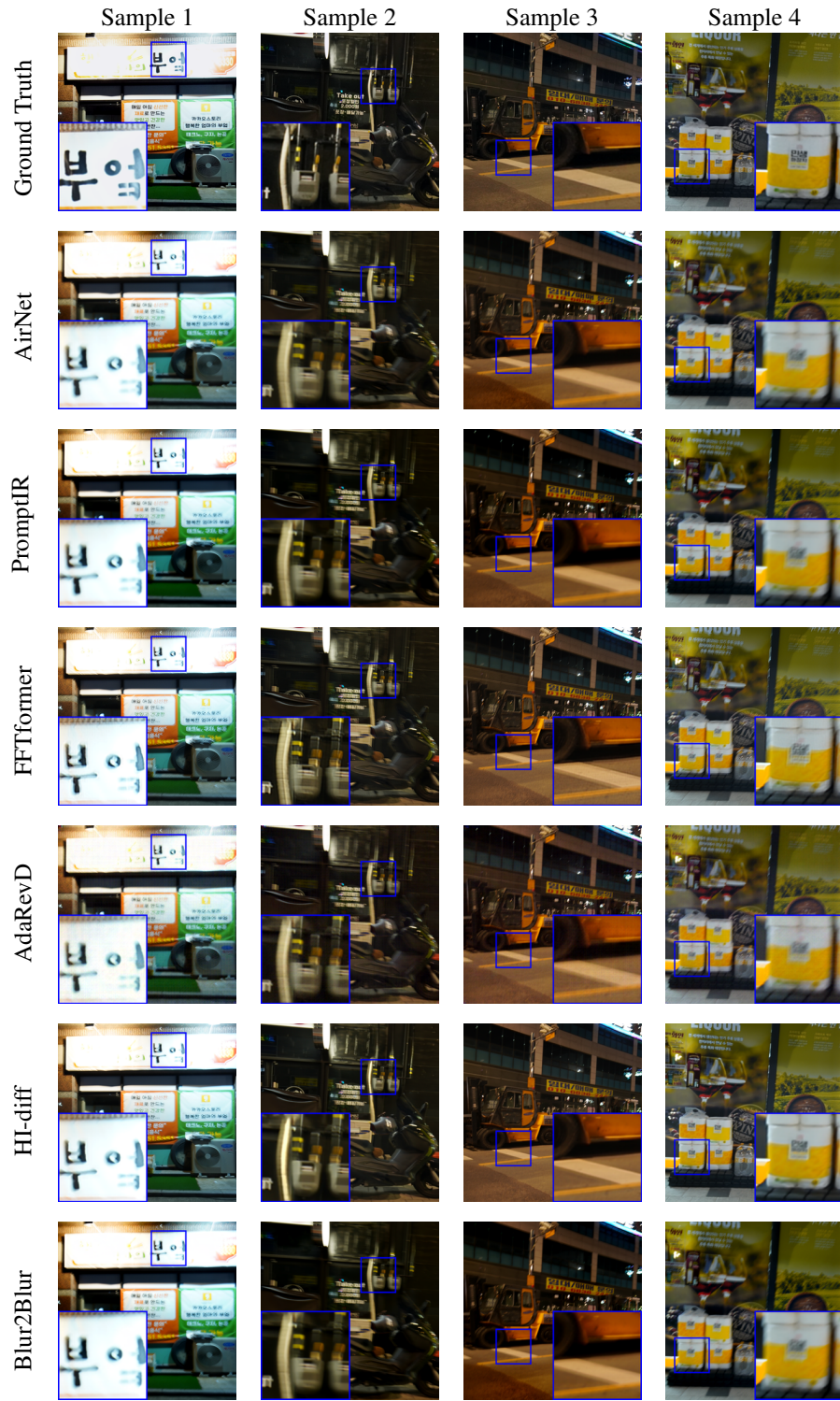


Figure 15: Additional visual comparison on the [RealBlur-J](#) dataset.

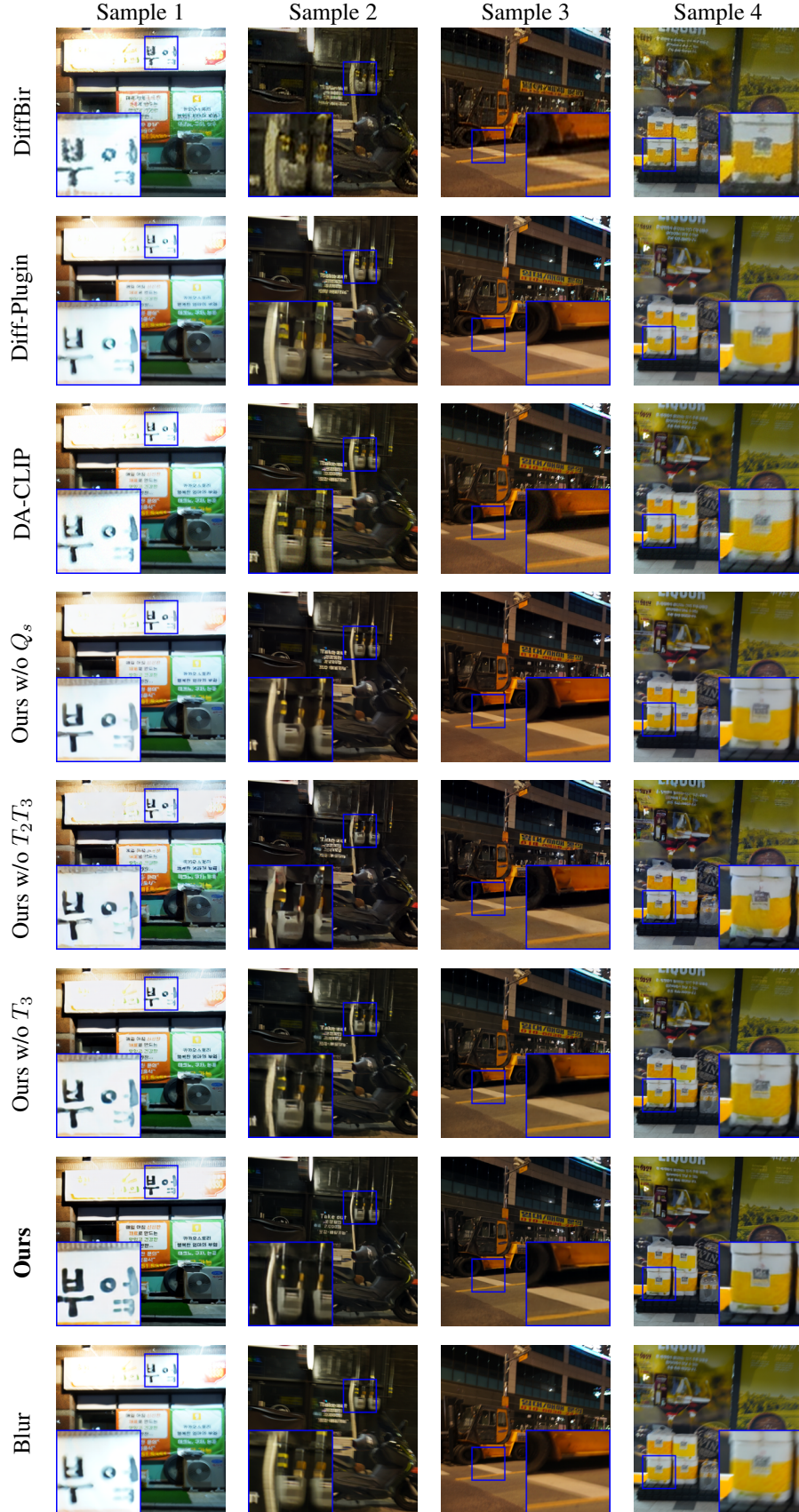


Figure 16: Additional visual comparison on the [RealBlur-J](#) dataset (Continue).

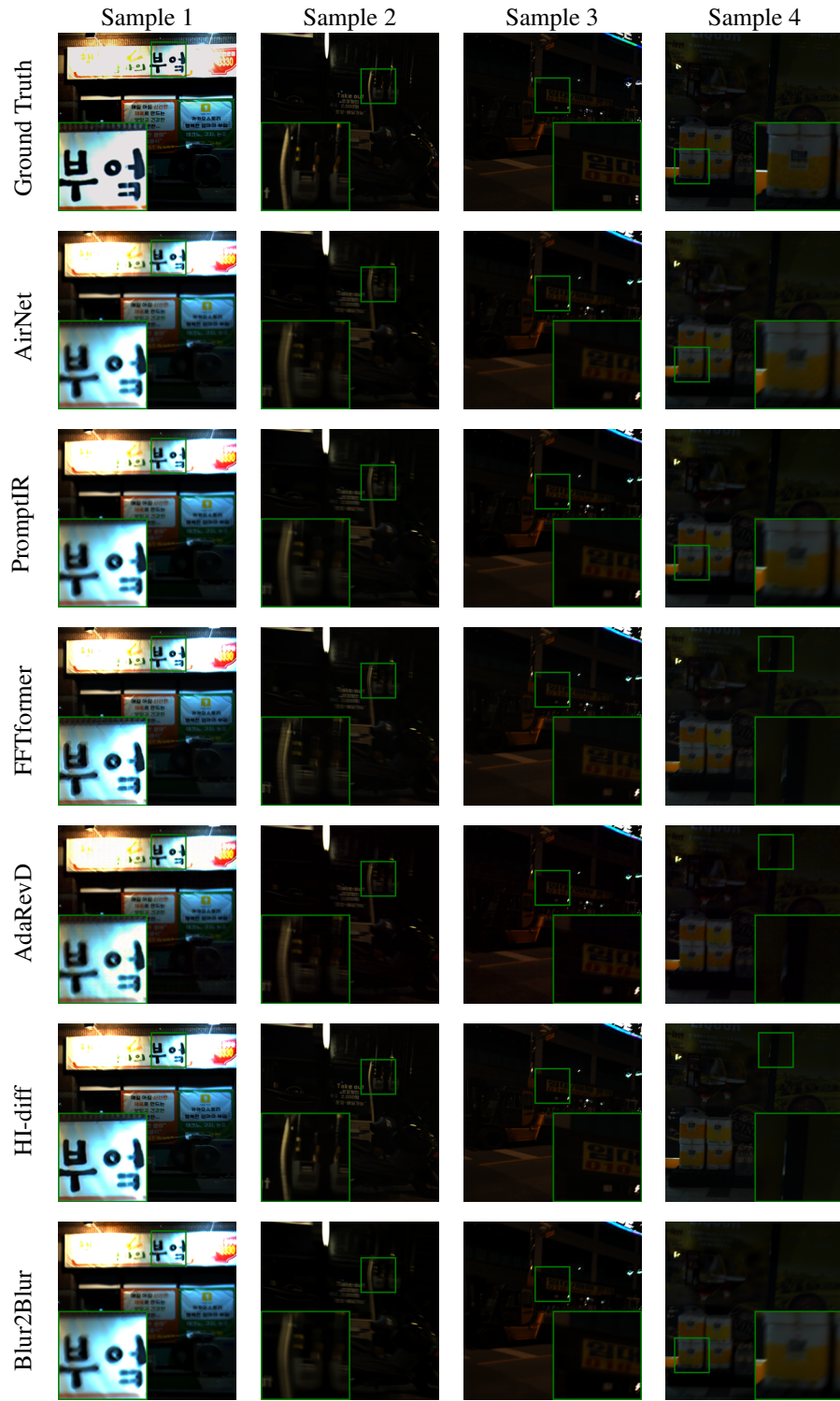


Figure 17: Additional visual comparison on the [RealBlur-R](#) dataset.

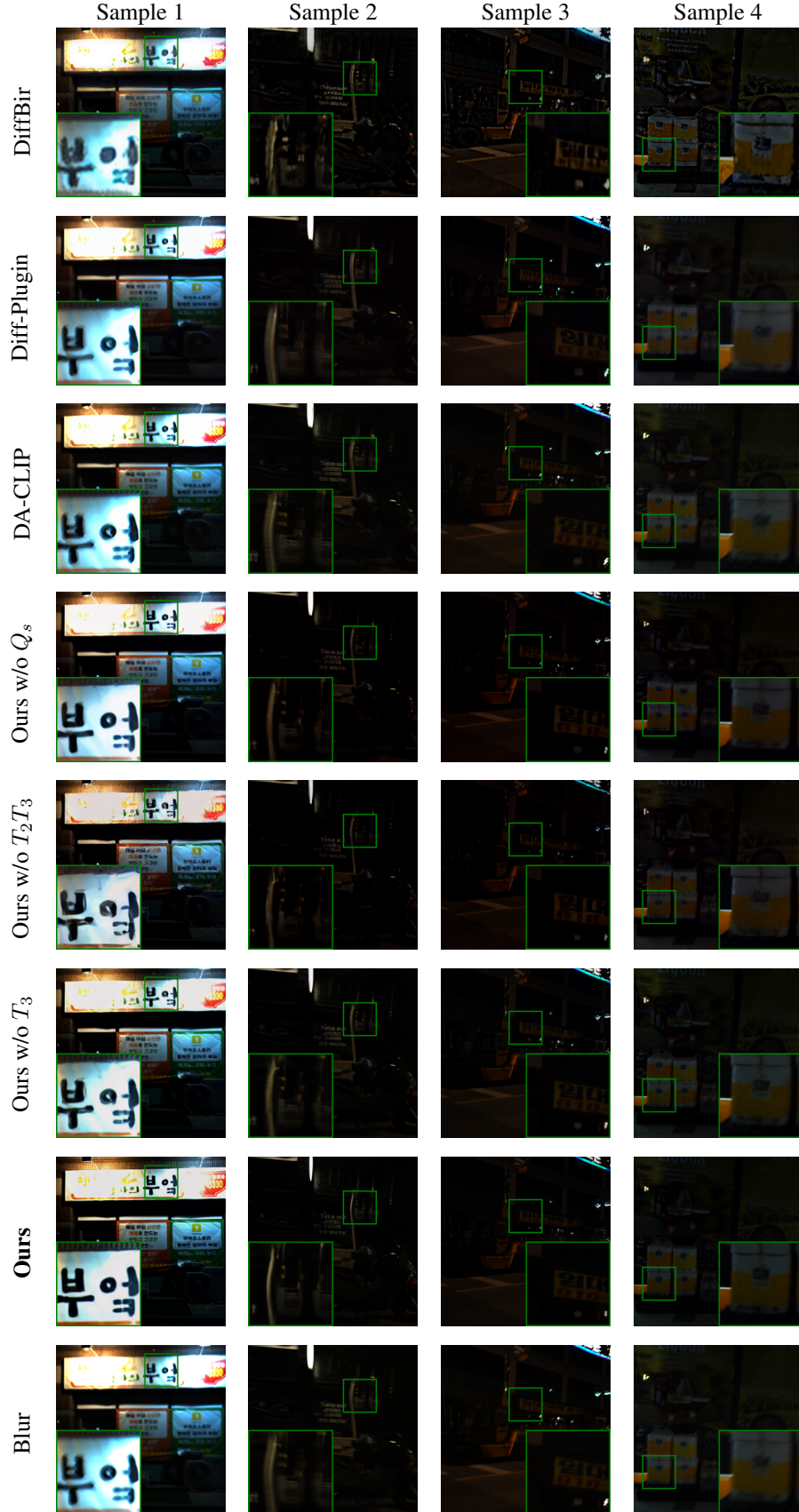


Figure 18: Additional visual comparison on the [RealBlur-R](#) dataset (Continue).

References

- [1] Youjian Zhang, Chaoyue Wang, and Dacheng Tao. Neural maximum a posteriori estimation on unpaired data for motion deblurring. IEEE Transactions on Pattern Analysis and Machine Intelligence, 2023. [1](#), [2](#), [3](#)
- [2] Bang-Dang Pham, Phong Tran, Anh Tran, Cuong Pham, Rang Nguyen, and Minh Hoai. Blur2blur: Blur conversion for unsupervised image deblurring on unknown domains. In Proceedings of the IEEE/CVF Conference on Computer Vision and Pattern Recognition, pages 2804–2813, 2024. [1](#), [2](#), [3](#), [4](#), [6](#), [7](#)
- [3] Kaihao Zhang, Wenhan Luo, Yiran Zhong, Lin Ma, Bjorn Stenger, Wei Liu, and Hongdong Li. Deblurring by realistic blurring. In Proceedings of the IEEE/CVF conference on computer vision and pattern recognition, pages 2737–2746, 2020. [1](#)
- [4] Xin Tao, Hongyun Gao, Xiaoyong Shen, Jue Wang, and Jiaya Jia. Scale-recurrent network for deep image deblurring. In Proceedings of the IEEE conference on computer vision and pattern recognition, pages 8174–8182, 2018. [1](#)
- [5] Seungjun Nah, Tae Hyun Kim, and Kyoung Mu Lee. Deep multi-scale convolutional neural network for dynamic scene deblurring. In Proceedings of the IEEE conference on computer vision and pattern recognition, pages 3883–3891, 2017. [1](#), [6](#)
- [6] Vaishnav Potlapalli, Syed Waqas Zamir, Salman H Khan, and Fahad Shahbaz Khan. Promptir: Prompting for all-in-one image restoration. Advances in Neural Information Processing Systems, 36, 2024. [1](#), [7](#)
- [7] Evelyn Chee and Zhenzhou Wu. Airnet: Self-supervised affine registration for 3d medical images using neural networks. arXiv preprint arXiv:1810.02583, 2018. [1](#), [7](#)
- [8] Orest Kupyn, Volodymyr Budzan, Mykola Mykhailych, Dmytro Mishkin, and Jiří Matas. Deblurgan: Blind motion deblurring using conditional adversarial networks. In Proceedings of the IEEE conference on computer vision and pattern recognition, pages 8183–8192, 2018. [1](#)
- [9] Shuang Zhang, Ada Zhen, and Robert L Stevenson. Gan based image deblurring using dark channel prior. arXiv preprint arXiv:1903.00107, 2019. [1](#)
- [10] Yuhong Zhang, Hengsheng Zhang, Xinning Chai, Zhengxue Cheng, Rong Xie, Li Song, and Wenjun Zhang. Diff-restorer: Unleashing visual prompts for diffusion-based universal image restoration. arXiv preprint arXiv:2407.03636, 2024. [1](#), [3](#), [6](#), [10](#)
- [11] Xinqi Lin, Jingwen He, Ziyan Chen, Zhaoyang Lyu, Bo Dai, Fanghua Yu, Yu Qiao, Wanli Ouyang, and Chao Dong. Diffbir: Toward blind image restoration with generative diffusion prior. In European Conference on Computer Vision, pages 430–448. Springer, 2025. [1](#), [3](#), [5](#), [6](#), [7](#)
- [12] Yuhao Liu, Zhanghan Ke, Fang Liu, Nanxuan Zhao, and Rynson WH Lau. Diff-plugin: Revitalizing details for diffusion-based low-level tasks. In Proceedings of the IEEE/CVF Conference on Computer Vision and Pattern Recognition, pages 4197–4208, 2024. [1](#), [3](#), [5](#), [7](#)
- [13] Jonathan Ho, Ajay Jain, and Pieter Abbeel. Denoising diffusion probabilistic models. Advances in neural information processing systems, 33:6840–6851, 2020. [1](#), [3](#)
- [14] Robin Rombach, Andreas Blattmann, Dominik Lorenz, Patrick Esser, and Björn Ommer. High-resolution image synthesis with latent diffusion models. In Proceedings of the IEEE/CVF conference on computer vision and pattern recognition, pages 10684–10695, 2022. [1](#), [3](#)
- [15] Zili Yi, Hao Zhang, Ping Tan, and Minglun Gong. Dualgan: Unsupervised dual learning for image-to-image translation. In Proceedings of the IEEE international conference on computer vision, pages 2849–2857, 2017. [2](#), [3](#)
- [16] Suiyi Zhao, Zhao Zhang, Richang Hong, Mingliang Xu, Yi Yang, and Meng Wang. Fel-gan: A lightweight and real-time baseline for unsupervised blind image deblurring. In Proceedings of the 30th ACM International Conference on Multimedia, pages 6220–6229, 2022. [2](#), [3](#)

- [17] DONG Jiangxin, S ROTH, and B SCHIELE. Learning spatially-variant map models for non-blind image deblurring [c]. the ieee. In CVF Conference on Computer Vision and Pattern Recognition, Nashville, USA, pages 4884–4893, 2021. [2](#), [3](#)
- [18] Dongwei Ren, Kai Zhang, Qilong Wang, Qinghua Hu, and Wangmeng Zuo. Neural blind deconvolution using deep priors. In Proceedings of the IEEE/CVF conference on computer vision and pattern recognition, pages 3341–3350, 2020. [2](#), [3](#)
- [19] Runhua Jiang and Yahong Han. Uncertainty-aware variate decomposition for self-supervised blind image deblurring. In Proceedings of the 31st ACM International Conference on Multimedia, pages 252–260, 2023. [2](#), [3](#)
- [20] Ian Goodfellow, Jean Pouget-Abadie, Mehdi Mirza, Bing Xu, David Warde-Farley, Sherjil Ozair, Aaron Courville, and Yoshua Bengio. Generative adversarial nets. Advances in neural information processing systems, 27, 2014. [2](#), [3](#)
- [21] Jia-Hao Wu, Fu-Jen Tsai, Yan-Tsung Peng, Chung-Chi Tsai, Chia-Wen Lin, and Yen-Yu Lin. Id-blau: Image deblurring by implicit diffusion-based reblurring augmentation. In Proceedings of the IEEE/CVF Conference on Computer Vision and Pattern Recognition, pages 25847–25856, 2024. [2](#), [3](#)
- [22] JunnanLi, Dongxu Li, Silvio Savarese, and Steven Hoi. Blip-2: Bootstrapping language-image pre-training with frozen image encoders and large language models. In International conference on machine learning, pages 19730–19742. PMLR, 2023. [2](#), [4](#)
- [23] Jascha Sohl-Dickstein, Eric Weiss, Niru Maheswaranathan, and Surya Ganguli. Deep unsupervised learning using nonequilibrium thermodynamics. In International conference on machine learning, pages 2256–2265. PMLR, 2015. [3](#)
- [24] Yang Song and Stefano Ermon. Generative modeling by estimating gradients of the data distribution. Advances in neural information processing systems, 32, 2019. [3](#)
- [25] Jiaming Song, Chenlin Meng, and Stefano Ermon. Denoising diffusion implicit models. arXiv: Learning, arXiv: Learning, Oct 2020. [3](#), [7](#)
- [26] Hu Ye, Jun Zhang, Sibio Liu, Xiao Han, and Wei Yang. Ip-adapter: Text compatible image prompt adapter for text-to-image diffusion models. arXiv preprint arXiv:2308.06721, 2023. [3](#), [5](#)
- [27] Junhao Cheng, Xi Lu, Hanhui Li, Khun Loun Zai, Baiqiao Yin, Yuhao Cheng, Yiqiang Yan, and Xiaodan Liang. Autostudio: Crafting consistent subjects in multi-turn interactive image generation. arXiv preprint arXiv:2406.01388, 2024. [3](#)
- [28] Xiangyang Luo, Junhao Cheng, Yifan Xie, Xin Zhang, Tao Feng, Zhou Liu, Fei Ma, and Fei Yu. Object isolated attention for consistent story visualization. arXiv preprint arXiv:2503.23353, 2025. [3](#)
- [29] Christoph Schuhmann, Romain Beaumont, Richard Vencu, Cade Gordon, Ross Wightman, Mehdi Cherti, Theo Coombes, Aarush Katta, Clayton Mullis, Mitchell Wortsman, et al. Laion-5b: An open large-scale dataset for training next generation image-text models. Advances in Neural Information Processing Systems, 35:25278–25294, 2022. [3](#)
- [30] Ilya Krylov, Sergei Nosov, and Vladislav Sovrasov. Open images v5 text annotation and yet another mask text spotter. In Asian Conference on Machine Learning, pages 379–389. PMLR, 2021. [3](#)
- [31] Prafulla Dhariwal and Alexander Nichol. Diffusion models beat gans on image synthesis. Advances in neural information processing systems, 34:8780–8794, 2021. [3](#)
- [32] Jonathan Ho and Tim Salimans. Classifier-free diffusion guidance. arXiv preprint arXiv:2207.12598, 2022. [3](#), [7](#)
- [33] Xingang Pan, Xiaohang Zhan, Bo Dai, Dahua Lin, Chen Change Loy, and Ping Luo. Exploiting deep generative prior for versatile image restoration and manipulation. IEEE Transactions on Pattern Analysis and Machine Intelligence, 44(11):7474–7489, 2021. [3](#)

- [34] Hyungjin Chung, Byeongsu Sim, Dohoon Ryu, and Jong Chul Ye. Improving diffusion models for inverse problems using manifold constraints. Advances in Neural Information Processing Systems, 35:25683–25696, 2022. 3
- [35] Yinhuai Wang, Jiwen Yu, and Jian Zhang. Zero-shot image restoration using denoising diffusion null-space model. arXiv preprint arXiv:2212.00490, 2022. 3
- [36] Hyungjin Chung, Jeongsol Kim, Michael T Mccann, Marc L Klasky, and Jong Chul Ye. Diffusion posterior sampling for general noisy inverse problems. arXiv preprint arXiv:2209.14687, 2022. 3
- [37] Bahjat Kawar, Michael Elad, Stefano Ermon, and Jiaming Song. Denoising diffusion restoration models. Advances in Neural Information Processing Systems, 35:23593–23606, 2022. 3
- [38] Haoying Li, Yifan Yang, Meng Chang, Shiqi Chen, Huajun Feng, Zhihai Xu, Qi Li, and Yueting Chen. Srdiff: Single image super-resolution with diffusion probabilistic models. Neurocomputing, 479:47–59, 2022. 3
- [39] Ozan Özdenizci and Robert Legenstein. Restoring vision in adverse weather conditions with patch-based denoising diffusion models. IEEE Transactions on Pattern Analysis and Machine Intelligence, 45(8):10346–10357, 2023. 3
- [40] Mengwei Ren, Mauricio Delbracio, Hossein Talebi, Guido Gerig, and Peyman Milanfar. Multiscale structure guided diffusion for image deblurring. In Proceedings of the IEEE/CVF International Conference on Computer Vision, pages 10721–10733, 2023. 3
- [41] Naoki Murata, Koichi Saito, Chieh-Hsin Lai, Yuhta Takida, Toshimitsu Uesaka, Yuki Mitsufuji, and Stefano Ermon. GibbsDDRM: A partially collapsed gibbs sampler for solving blind inverse problems with denoising diffusion restoration. In International Conference on Machine Learning, 2023. 3
- [42] Hanting Chen, Yunhe Wang, Tianyu Guo, Chang Xu, Yiping Deng, Zhenhua Liu, Siwei Ma, Chunjing Xu, Chao Xu, and Wen Gao. Pre-trained image processing transformer. arXiv, 2021. 3
- [43] Hyungjin Chung, Jeongsol Kim, Sehui Kim, and Jong Chul Ye. Parallel diffusion models of operator and image for blind inverse problems. IEEE/CVF Conference on Computer Vision and Pattern Recognition, 2023. 3
- [44] Jianyi Wang, Zongsheng Yue, Shangchen Zhou, Kelvin CK Chan, and Chen Change Loy. Exploiting diffusion prior for real-world image super-resolution. International Journal of Computer Vision, pages 1–21, 2024. 3
- [45] Ziwei Luo, Fredrik K Gustafsson, Zheng Zhao, Jens Sjölund, and Thomas B Schön. Controlling vision-language models for universal image restoration. arXiv preprint arXiv:2310.01018, 3(8), 2023. 3, 7
- [46] Lingshun Kong, Jiawei Zhang, Dongqing Zou, Jimmy Ren, Xiaohe Wu, Jiangxin Dong, and Jinshan Pan. Deblurdiff: Real-world image deblurring with generative diffusion models, 2025. 3
- [47] Dan Hendrycks and Thomas Dietterich. Benchmarking neural network robustness to common corruptions and perturbations. arXiv preprint arXiv:1903.12261, 2019. 3, 5
- [48] Jaesung Rim, Geonung Kim, Jungeon Kim, Junyong Lee, Seungyong Lee, and Sunghyun Cho. Realistic blur synthesis for learning image deblurring. In European conference on computer vision, pages 487–503. Springer, 2022. 3
- [49] Liangyu Chen, Xiaojie Chu, Xiangyu Zhang, and Jian Sun. Simple baselines for image restoration. In European conference on computer vision, pages 17–33. Springer, 2022. 3
- [50] Sung-Jin Cho, Seo-Won Ji, Jun-Pyo Hong, Seung-Won Jung, and Sung-Jea Ko. Rethinking coarse-to-fine approach in single image deblurring. In Proceedings of the IEEE/CVF international conference on computer vision, pages 4641–4650, 2021. 3

- [51] Dasong Li, Yi Zhang, Ka Chun Cheung, Xiaogang Wang, Hongwei Qin, and Hongsheng Li. Learning degradation representations for image deblurring. In European conference on computer vision, pages 736–753. Springer, 2022. 3
- [52] Xintian Mao, Yiming Liu, Fengze Liu, Qingli Li, Wei Shen, and Yan Wang. Intriguing findings of frequency selection for image deblurring. In Proceedings of the AAAI Conference on Artificial Intelligence, volume 37, pages 1905–1913, 2023. 3
- [53] Fu-Jen Tsai, Yan-Tsung Peng, Yen-Yu Lin, Chung-Chi Tsai, and Chia-Wen Lin. Stripformer: Strip transformer for fast image deblurring. In European conference on computer vision, pages 146–162. Springer, 2022. 3
- [54] Lingshun Kong, Jiangxin Dong, Jianjun Ge, Mingqiang Li, and Jinshan Pan. Efficient frequency domain-based transformers for high-quality image deblurring. In Proceedings of the IEEE/CVF Conference on Computer Vision and Pattern Recognition, pages 5886–5895, 2023. 3
- [55] Pengwei Liang, Junjun Jiang, Xianming Liu, and Jiayi Ma. Image deblurring by exploring in-depth properties of transformer. IEEE Transactions on Neural Networks and Learning Systems, 2024. 3
- [56] Hanzhou Liu, Binghan Li, Chengkai Liu, and Mi Lu. Deblurdinat: A lightweight and effective transformer for image deblurring. arXiv preprint arXiv:2403.13163, 2024. 3
- [57] Zhenxuan Fang, Fangfang Wu, Weisheng Dong, Xin Li, Jinjian Wu, and Guangming Shi. Self-supervised non-uniform kernel estimation with flow-based motion prior for blind image deblurring. In Proceedings of the IEEE/CVF conference on computer vision and pattern recognition, pages 18105–18114, 2023. 3
- [58] Chengxu Liu, Xuan Wang, Xiangyu Xu, Ruhao Tian, Shuai Li, Xueming Qian, and Ming-Hsuan Yang. Motion-adaptive separable collaborative filters for blind motion deblurring. In Proceedings of the IEEE/CVF Conference on Computer Vision and Pattern Recognition, pages 25595–25605, 2024. 3
- [59] Zheng Chen, Yulun Zhang, Ding Liu, Jinjin Gu, Linghe Kong, Xin Yuan, et al. Hierarchical integration diffusion model for realistic image deblurring. Advances in neural information processing systems, 36, 2024. 3
- [60] Charles Laroche, Andrés Almansa, and Eva Coupete. Fast diffusion em: a diffusion model for blind inverse problems with application to deconvolution. In Proceedings of the IEEE/CVF Winter Conference on Applications of Computer Vision, pages 5271–5281, 2024. 3
- [61] Jiangxin Dong, Stefan Roth, and Bernt Schiele. Learning spatially-variant map models for non-blind image deblurring. In Proceedings of the IEEE/CVF conference on computer vision and pattern recognition, pages 4886–4895, 2021. 3
- [62] Diederik P Kingma. Auto-encoding variational bayes. arXiv preprint arXiv:1312.6114, 2013. 3
- [63] Dongxu Li, Junnan Li, and Steven Hoi. Blip-diffusion: Pre-trained subject representation for controllable text-to-image generation and editing. Advances in Neural Information Processing Systems, 36, 2024. 4, 7
- [64] Junhao Cheng, Baiqiao Yin, Kaixin Cai, Minbin Huang, Hanhui Li, Yuxin He, Xi Lu, Yue Li, Yifei Li, Yuhao Cheng, et al. Theatergen: Character management with llm for consistent multi-turn image generation. arXiv preprint arXiv:2404.18919, 2024. 5
- [65] Bohao Peng, Jian Wang, Yuechen Zhang, Wenbo Li, Ming-Chang Yang, and Jiaya Jia. Controlnext: Powerful and efficient control for image and video generation. arXiv preprint arXiv:2408.06070, 2024. 5
- [66] Lvmin Zhang, Anyi Rao, and Maneesh Agrawala. Adding conditional control to text-to-image diffusion models. In Proceedings of the IEEE/CVF International Conference on Computer Vision, pages 3836–3847, 2023. 5

- [67] Chong Mou, Xintao Wang, Liangbin Xie, Yanze Wu, Jian Zhang, Zhongang Qi, and Ying Shan. T2i-adapter: Learning adapters to dig out more controllable ability for text-to-image diffusion models. In Proceedings of the AAAI Conference on Artificial Intelligence, 2024. 5
- [68] Alec Radford, Jong Wook Kim, Chris Hallacy, Aditya Ramesh, Gabriel Goh, Sandhini Agarwal, Girish Sastry, Amanda Askell, Pamela Mishkin, Jack Clark, et al. Learning transferable visual models from natural language supervision. In International conference on machine learning, pages 8748–8763. PMLR, 2021. 5, 7
- [69] Dar-Yen Chen, Hamish Tennent, and Ching-Wen Hsu. Artadapter: Text-to-image style transfer using multi-level style encoder and explicit adaptation. In Proceedings of the IEEE/CVF Conference on Computer Vision and Pattern Recognition, pages 8619–8628, 2024. 5
- [70] I Chen, Wei-Ting Chen, Yu-Wei Liu, Yuan-Chun Chiang, Sy-Yen Kuo, Ming-Hsuan Yang, et al. Unirestore: Unified perceptual and task-oriented image restoration model using diffusion prior. arXiv preprint arXiv:2501.13134, 2025. 6, 10
- [71] Jaesung Rim, Haeyun Lee, Jucheol Won, and Sunghyun Cho. Real-world blur dataset for learning and benchmarking deblurring algorithms. In Computer Vision–ECCV 2020: 16th European Conference, Glasgow, UK, August 23–28, 2020, Proceedings, Part XXV 16, pages 184–201. Springer, 2020. 6
- [72] Seungjun Nah, Sungyong Baik, Seokil Hong, Gyeongsik Moon, Sanghyun Son, Radu Timofte, and Kyoung Mu Lee. Ntire 2019 challenge on video deblurring and super-resolution: Dataset and study. In Proceedings of the IEEE/CVF conference on computer vision and pattern recognition workshops, pages 0–0, 2019. 6
- [73] Sidi Yang, Tianhe Wu, Shuwei Shi, Shanshan Lao, Yuan Gong, Mingdeng Cao, Jiahao Wang, and Yujiu Yang. Maniqa: Multi-dimension attention network for no-reference image quality assessment. In Proceedings of the IEEE/CVF Conference on Computer Vision and Pattern Recognition, pages 1191–1200, 2022. 6
- [74] Weixia Zhang, Guangtao Zhai, Ying Wei, Xiaokang Yang, and Kede Ma. Blind image quality assessment via vision-language correspondence: A multitask learning perspective. In Proceedings of the IEEE/CVF conference on computer vision and pattern recognition, pages 14071–14081, 2023. 6
- [75] Junjie Ke, Qifei Wang, Yilin Wang, Peyman Milanfar, and Feng Yang. Musiq: Multi-scale image quality transformer. In Proceedings of the IEEE/CVF international conference on computer vision, pages 5148–5157, 2021. 6
- [76] Jianyi Wang, Kelvin CK Chan, and Chen Change Loy. Exploring clip for assessing the look and feel of images. In Proceedings of the AAAI Conference on Artificial Intelligence, 2023. 6
- [77] I Loshchilov. Decoupled weight decay regularization. arXiv preprint arXiv:1711.05101, 2017. 7
- [78] Qingli Li Xintian Mao and Yan Wang. Adarevd: Adaptive patch exiting reversible decoder pushes the limit of image deblurring. In Proc. CVPR, 2024. 7
- [79] Lingshun Kong, Jiangxin Dong, Mingqiang Li, Jianjun Ge, and Jinshan Pan. Efficient frequency domain-based transformers for high-quality image deblurring, 2022. 7
- [80] Zheng Chen, Yulun Zhang, Liu Ding, Xia Bin, Jinjin Gu, Linghe Kong, and Xin Yuan. Hierarchical integration diffusion model for realistic image deblurring. In NeurIPS, 2023. 7
- [81] Zixin Zhu, Xuelu Feng, Dongdong Chen, Jianmin Bao, Le Wang, Yinpeng Chen, Lu Yuan, and Gang Hua. Designing a better asymmetric vqgan for stablediffusion. arXiv preprint arXiv:2306.04632, 2023. 10
- [82] Richard Zhang, Phillip Isola, Alexei A Efros, Eli Shechtman, and Oliver Wang. The unreasonable effectiveness of deep features as a perceptual metric. In Proceedings of the IEEE conference on computer vision and pattern recognition, pages 586–595, 2018. 10